

Full Length Article

Experimental study on the CH₄/CO₂ competitive adsorption behaviors of typical shale minerals in low pressure reservoirsSen Tian ^{a,d,*}, Huimin Jia ^a, Zhaolong Ge ^a, Guangjin Wang ^b, Ruyi Bai ^{a,c}^a State Key Laboratory of Coal Mine Disaster Dynamics and Control, School of Resources and Safety Engineering, Chongqing University, Chongqing 400044, China^b Faculty of Land Resources Engineering, Kunming University of Science and Technology, Kunming 650093, China^c Xi'an Aerospace Chemical Power Co., Ltd, Xi'an 710511, China^d School of Civil Engineering, The University of Queensland, Brisbane, QLD 4072, Australia

ARTICLE INFO

ABSTRACT

Keywords:

Shale gas
Low pressure reservoirs
Competitive adsorption
Adsorption experiment
Pore structure

With the large-scale exploitation of shale gas resources, there are more and more shale gas wells with pressure exhaustion and even abandonment in low pressure reservoirs. However, these shale gas wells are rich in resources and still have great exploitation potential and utilization value. On this basis, the basic physical parameters of typical shale minerals (montmorillonite, calcite, and illite), such as pore structure, were investigated through carrying out low temperature nitrogen test based on field research and mineral composition tests. Meanwhile, by performing the volumetric method adsorption experiment, the competitive adsorption behavioral characteristics of minerals under the conditions of temperature at 70–130°C, pressure at 0–6 MPa and different gas mixture ratios of CH₄/CO₂ were studied. In addition, the key influencing factors and rules of the competitive adsorption of typical shale minerals under the high temperature and low pressure conditions were revealed. The results showed that under the experimental conditions, the lower temperature and the higher pressure led to the larger adsorption capacities of three minerals, and the growth rate of adsorption capacity gradually slowed down with the increase in pressure. To be specific, the order of minerals adsorption capacity montmorillonite > calcite > illite, proved that the larger mineral specific surface area resulted in the larger pore volume, the better pore structure development, and the superior adsorption performance. At the optimal adsorption effect (70°C, 6 MPa, 75 %CO₂ + 25 %CH₄), the adsorption capacity of montmorillonite was 0.381 mmol/g, while that of illite was 0.085 mmol/g, and that of calcite was 0.164 mmol/g. Because carbon dioxide occupied most of the adsorption sites and spaces on the surfaces of the three minerals during their competitive adsorption, carbon dioxide had stronger competitive adsorption performance. The results in this study prove to a certain extent that under the low pressure and high temperature conditions, increasing the carbon dioxide concentration is more conducive to shale gas displacement, so as to improve the shale gas recovery rate.

1. Introduction

The development of global energy has entered a critical period of transition from fossil fuels to renewable energy sources [1]. Shale gas, as a substantial unconventional natural gas resource, is of great significance in alleviating the supply–demand contradiction of natural gas, bridging the energy gap, optimizing the energy structure, and ensuring energy supply and security. The globally recoverable shale gas resources amount to approximately $220.6 \times 10^{12} \text{ m}^3$ [2], yet only a few countries have achieved commercial development to date. Similar to conventional energy sources such as coal and petroleum, with the large-scale

exploitation and utilization of shale gas resources, the number of depleted shale gas wells in low-pressure reservoirs will gradually increase [3]. These wells still contain abundant residual resources and possess considerable potential for further development and utilization [4]. However, research on the fundamental theories and methodologies for shale gas development in low-pressure environments remains relatively less. Currently, shale gas development commonly employs horizontal drilling technology [5], simultaneous fracturing [6], and staged fracturing techniques [7,8]. Among these, CO₂-enhanced shale gas recovery (CO₂-EGR) has emerged as a research hotspot in the field of shale gas extraction due to its advantages of high recovery rates, shortened

* Corresponding author at: State Key Laboratory of Coal Mine Disaster Dynamics and Control, School of Resources and Safety Engineering, Chongqing University, Chongqing 400044, China.

E-mail address: sentian@cqu.edu.cn (S. Tian).

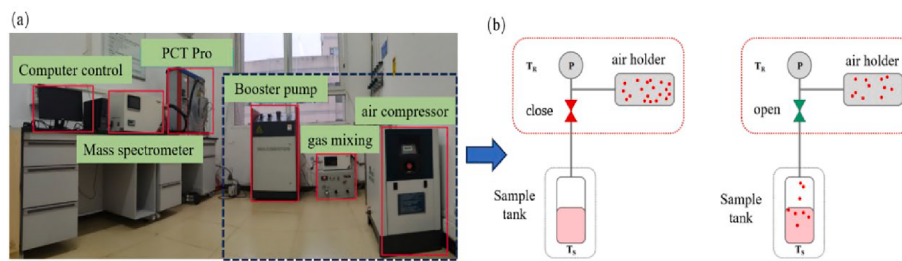


Fig. 1. Adsorption experimental equipment (a) Volumetric method experimental equipment; (b) Principle of adsorption equilibrium process.

production cycles, and contributions to geological carbon dioxide sequestration [9].

The adsorption capacity of shale gas is influenced by various factors, which are generally categorized into external and internal factors. External factors include temperature, pressure, and stratigraphic depth, while internal factors encompass mineral composition, total organic carbon (TOC) content, organic matter maturity, as well as water content and porosity [10–12]. The experimental studies on isotherm adsorption on different clay rich rocks indicate that different mineral compositions of shale exhibit significant effects on methane adsorption capacity. As discovered from X-ray diffraction (XRD) analysis, the illite, montmorillonite and calcite are the key components, which play a vital role in gas adsorption in shale bed [13,14]. Ma et al. [14] have observed that among clay minerals, montmorillonite demonstrates the strongest adsorption capacity, followed by illite/smectite mixed layers, kaolinite, chlorite, and illite. Yang et al. [15] evaluated the impact of shale clay minerals on gas adsorption behavior and found that clay minerals contribute 16 to 47 % to methane adsorption capacity; They also discovered a positive correlation between quartz content and methane adsorption capacity in the Longmaxi Formation shale of Sichuan [15]. Furthermore, some scholars have found that a higher TOC content in shale results in a greater saturated adsorption capacity for methane [16,17]. Among external factors, temperature and pressure directly affect the molecular kinetic energy of shale gas, thereby influencing its adsorption properties on mineral surfaces [18,19]. Chalmers et al. [20] suggested a possible negative power-law relationship between temperature and methane adsorption capacity, indicating a decline in methane adsorption capacity with increasing temperature. Additionally, scholars have investigated the influence of water on shale adsorption capacity and adsorption patterns, finding that as the relative humidity of shale increases, its adsorption capacity initially decreases significantly, as water molecules more easily occupy the adsorption space on mineral surfaces compared to methane [21]. Under high-pressure conditions, methane adsorption capacity enhances with increasing pressure in shale reservoirs [22,23].

In terms of research methods, isothermal adsorption experiment and macro/micro simulation are mainly used at present [24]. The adsorption capacity and influencing factors of CH₄/CO₂ under different conditions were characterized by carrying out the laboratory adsorption experiment methods of gravimetric method and volumetric method [25,26]. At the same time, many researchers have used molecular mechanics (MM) [27,28], molecular dynamics (MD) [29,30], Monte Carlo (GCMC) [31,32] and other molecular simulation methods to study the gas adsorption capacity and distribution effect of shale reservoirs under different geological depths [33]. The pore structure parameters were obtained by density functional theory (DFT) [34] and Barrett-Joyner-Halenda (BJH) [35], BET [36] and Langmuir [37], and the adsorption-diffusion behavior of CH₄, CO₂, ethane and other gases in different minerals under different temperature, pressure and pore size conditions was analysed [38]. In summary, the influencing factors of shale gas adsorption characteristics are complex, but most of the current studies focus on the adsorption effect under a single condition, and a mature influencing factor system has not been formed. In addition, there are few

studies on the competitive adsorption characteristics of mixed gases, especially for the competitive adsorption effect of CH₄/CO₂ in shale minerals under low pressure environment, further exploration is needed.

Therefore, to improve the shale gas well recovery rate and the collaborative utilization of space resources, this paper selected three shale minerals, namely, montmorillonite, illite and calcite, as the objects of study, obtained the adsorption isotherms of these three minerals through low temperature nitrogen test, and analyzed the pore structures, shapes and distribution characteristics of the three minerals according to the IUPAC standards. Additionally, the key basic physical parameters such as specific surface area, pore volume and pore size distribution of minerals were analyzed in line with the adsorption theories like BET and BJH. On this basis, the volumetric laboratory adsorption experiment was performed to study the competitive adsorption behavior characteristics of minerals under the conditions of temperature at 70–130°C, pressure at 0–6 MPa and different gas mixture ratios of CH₄/CO₂. Furthermore, the key influencing factors and rules of competitive adsorption of typical shale minerals under the high temperature and low pressure conditions were also revealed. This study may provide theoretical foundation and basic data for the application of the CO₂ displacement of shale gas technology in the low pressure environment.

2. Experimental methods

2.1. Low temperature nitrogen adsorption experiments

In this paper, montmorillonite, illite and calcite were analyzed by low-temperature nitrogen adsorption method suitable for 2–50 nm pore size, and the pore structure characteristics of minerals such as specific surface area and pore volume were obtained.

When the relative pressure P/P₀ exceeds 0.4, the pore volume can be determined by measuring the volume of injected liquid nitrogen, and the pore size distribution can be analyzed using the BJH method based on Kelvin equation. The equations are as follows [39,40]:

$$\ln \frac{P}{P_0} = \frac{2\gamma V_1}{rRT} \cos\theta \quad (1)$$

$$r = -2 \times 10^9 \gamma V_0 / [RT \ln(P/P_0)] + 0.354[-5/\ln(P/P_0)]^{1/3} \quad (2)$$

P: partial pressure of nitrogen, P_A; P₀: saturated vapor pressure of nitrogen, P_A; γ : surface tension of liquid nitrogen, n/m; V₁: molar volume of liquid; θ : wetting angle, °; r: molar heat capacity, J/(K·mol); T: temperature, K; R: pore size, nm; V₀: adsorption volume of the monolayer, cm³/g.

2.2. Competitive adsorption experiments

2.2.1. Volumetric adsorption experiments

The volumetric method is based on the equation of state of gas, and the adsorption capacity was calculated by calculating the change of free space volume (Fig. 1). The specific gas state equation is shown below [41].

Table 1

Experimental parameters of volumetric method adsorption experiment.

Buried depth/ km	Temperature/ °C	Gas ratio (CH ₄ + CO ₂)	Stress/ MPa
2	70	25 %+75 %	0~6
		50 %+50 %	
		75 %+25 %	
3	100	25 %+75 %	
		50 %+50 %	
		75 %+25 %	
4	130	25 %+75 %	
		50 %+50 %	
		75 %+25 %	

$$NRT = P_1 V_1 + P_2 V_2 - P_3 V_3 - P_4 V_4 \quad (3)$$

N: amount of adsorbate, mol; *T*: temperature, °C; *R*: Gas constant; *P*₁: gas tank pressure before adsorption, MPa; *V*₁: gas volume of gas tank before adsorption, cm³; *P*₂: sample tank pressure before adsorption, MPa; *V*₂: free space volume of sample tank before adsorption, cm³; *P*₃: gas tank pressure after adsorption equilibrium, MPa; *V*₃: gas volume of gas tank after adsorption equilibrium, cm³; *P*₄: gas pressure of sample tank after adsorption equilibrium, MPa; *V*₄: free space volume of sample tank after adsorption equilibrium, cm³; after adsorption equilibrium, *P*₃ and *P*₄ are equal.

2.2.2. Competitive adsorption parameters

Since the main burial depth of shale gas of the research subject in southwest China is 2–4 km, the burial depth of 2 km, 3 km and 4 km were selected equidistant and the corresponding temperatures were calculated. The temperature gradient is 30 k/km, and the equation of burial temperature is shown below [4].

$$T_{\log} = T_0 + \frac{DEP \times D}{100} \quad (4)$$

*T*_{log}: buried depth temperature, K; *T*₀: surface temperature, K; *D*: temperature gradient, K/100 m; *DEP*: buried depth, m.

The waste pressures can be calculated through Eq. (5)[4,42].

$$P = 0.3515 + 0.0010713 \times D \quad (5)$$

P: waste pressure, MPa; *D*: well depth, m.

According to the buried depth of 2–4 km, the waste pressure is 2.5 MPa, 3.56 MPa and 4.6 MPa, respectively. Therefore, the experimental pressure condition was set to 0–6 MPa. At the same time, different CH₄/CO₂ mixing ratios were selected to explore the competitive adsorption characteristics of the three minerals for CH₄/CO₂, respectively. The specific experimental parameters are shown in Table 1.

3. Results and discussions

3.1. Basic physical parameters and characteristics

3.1.1. Adsorption/desorption isothermal curves of minerals

Fig. 2 shows the retention loop curves of three minerals in the low-temperature nitrogen experiment. Among them, the adsorption curve of montmorillonite shows IUPAC adsorption isotherm IV curve. In the early period of adsorption ($0 < p/p_0 < 0.4$), the adsorption curve shows an upward convex shape. In the middle period of adsorption ($0.4 < p/p_0 < 0.8$), the mesopores in montmorillonite produce capillary condensation phenomenon, and the adsorption curve increases rapidly. In the later period of adsorption ($0.8 < p/p_0 < 1.0$), the curve has an inflection point, and the retention loop has an end point. It is seen that the montmorillonite sample is mainly composed of mesopores and macropores. Similarly, the adsorption curve of illite belongs to the III curve type, and its material is macroporous sheet-like particle structure, with incomplete pore structure and narrow pores; The adsorption curve of calcite is more similar to that of type IV, and its pores are mostly slit type with good connectivity. Therefore, in the low-temperature nitrogen

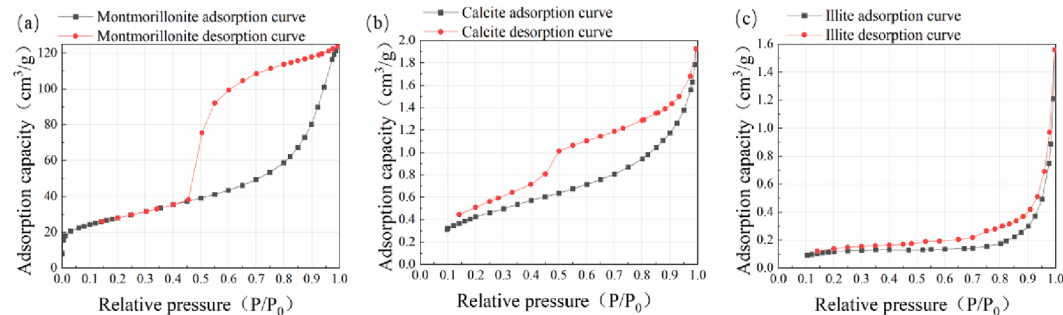


Fig. 2. Retention loop curves of minerals in the low-temperature nitrogen experiment. (a) montmorillonite; (b) calcite; (c) illite.

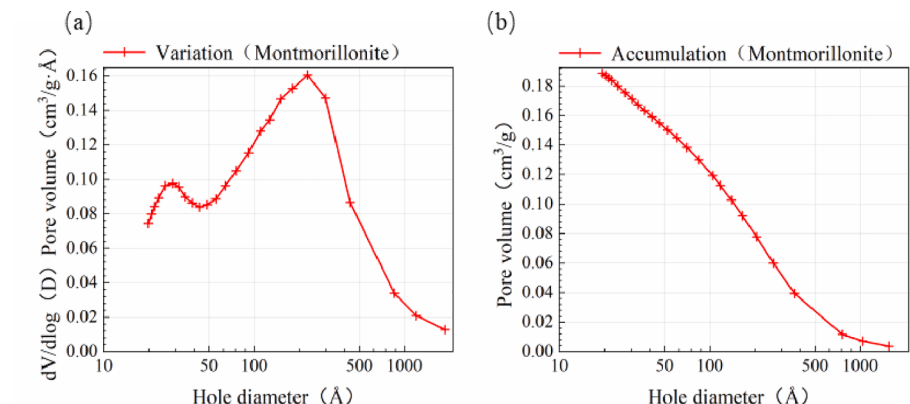


Fig. 3. Relation between pore diameter and pore volume of montmorillonite (a) variation; (b) accumulation.

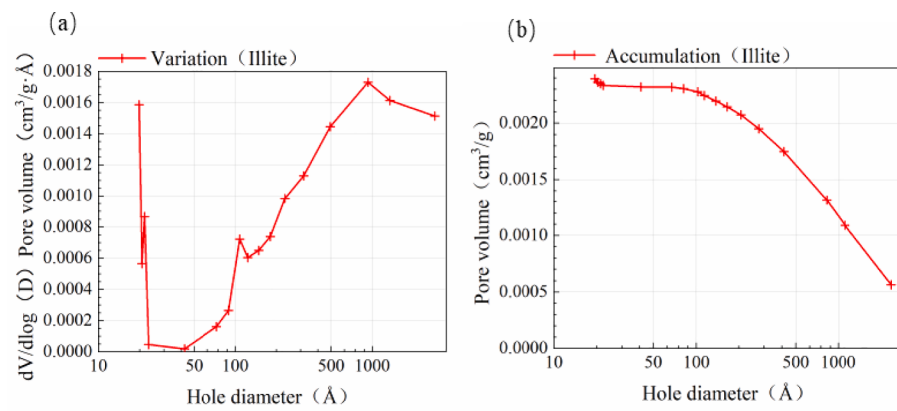


Fig. 4. Relation between pore diameter and pore volume of illite (a) variation; (b) accumulation.

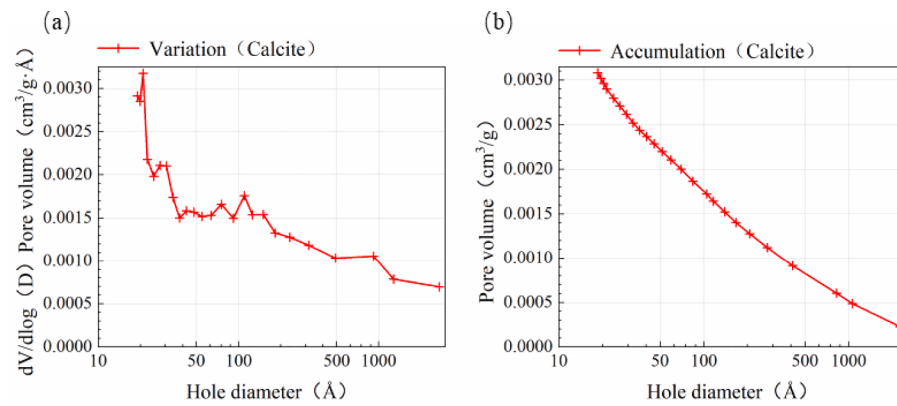


Fig. 5. Relation between pore diameter and pore volume of the calcite (a) variation; (b) accumulation.

experiment, the adsorption capacity of minerals for nitrogen is montmorillonite > calcite > illite.

3.1.2. Pore distribution of minerals

Fig. 3 shows the relations between pore diameter and pore volume of montmorillonite. In Fig. 3(a), there are two peaks around the pore diameter of 30 \AA and 250 \AA , and both belong to the mesoporous size, indicating that the mesoporous pores in montmorillonite have a significant effect on its pore volume. In Fig. 3(b), when the pore size is less than 500 \AA , the cumulative pore volume of montmorillonite decreases rapidly with the increase of pore size; when the pore size exceeded 500 \AA , the reduction trend of pore volume slowed down. It can be seen that mesopores are the main pore structure in montmorillonite samples, providing a larger storage space for shale gas.

In Fig. 4(a), there are three peaks, which are located in the pore size range of 15–20 \AA , 100–120 \AA , and 800–1000 \AA ; In Fig. 4(b), the cumulative pore volume decreases with the increase of pore diameter. It shows that micropores and macropores account for the main pore volume distribution in illite samples, while mesopores account for the smallest proportion.

Fig. 5 shows the curve variations of pore diameter and pore volume of the calcite. There are multiple peaks in the curve, and the most obvious three pore diameters are 15–20 \AA , 25–35 \AA , and 100–200 \AA , indicating that the well-developed pores of calcite are concentrated in 0–500 \AA . In Fig. 5 (b), the pore accumulation count of calcite shows a downward trend with the expansion of pore size. Therefore micropores and mesopores contribute more to the pore structure of calcite.

The pore volume of montmorillonite is significantly larger than that of calcite and illite, and illite is the smallest. The analysis shows that the specific surface area and total pore volume of montmorillonite and

Table 2
Experimental parameters of volumetric method.

Minerals	BET surface area (m^2/g)	Langmuir Specific surface area (m^2/g)	BJH Specific surface area (m^2/g)	Average pore size (nm)	BJH Total adsorption pore volume (cm^3/g)
montmorillonite	97.7549	153.2074	87.7600	8.5946	0.188567
illite	0.4047	0.6964	0.3340	28.6912	0.002394
calcite	1.6558	2.9846	1.7630	6.9948	0.003083

calcite are mainly from mesopores and micropores, while the specific surface area and pore volume of illite are mainly composed of macropores and micropores. In addition, montmorillonite has a more neat pore size distribution structure, the pore structure is well developed and concentrated, and the more evenly distributed pore size can provide more adsorption sites to enhance the adsorption capacity.

3.1.3. Specific surface area and pore volume of minerals

The specific surface areas, average pore sizes and total adsorption pore volumes of the three minerals were obtained by low-temperature nitrogen adsorption experiments (Table 2).

According to the analysis table, the specific surface area of montmorillonite is larger than that of illite and calcite. The larger the specific surface area of minerals, the more solid surface adsorption sites contacted by gas molecules can be provided, and the stronger the adsorption capacity. At the same time, the total pore volume: montmorillonite > calcite > illite. There is a positive correlation between the pore volume of minerals and their adsorption capacity.

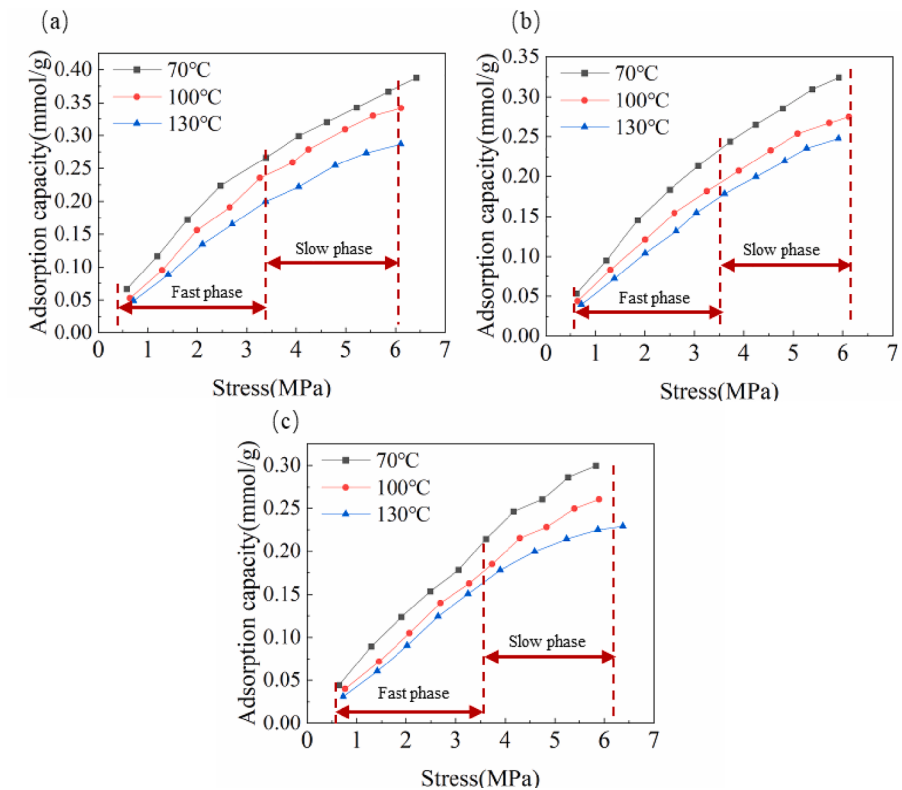


Fig. 6. Adsorption capacity of different gas ratio of CH_4/CO_2 in montmorillonite (a) 75 % $\text{CO}_2 + 25\% \text{CH}_4$; (b) 50 % $\text{CO}_2 + 50\% \text{CH}_4$; (c) 25 % $\text{CO}_2 + 75\% \text{CH}_4$.

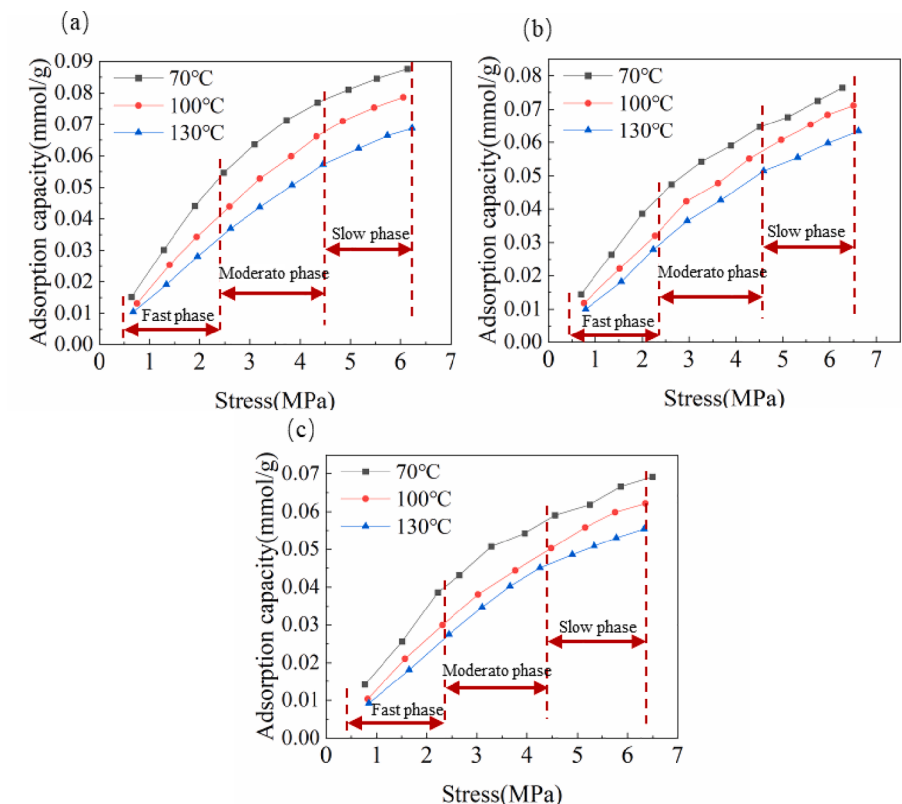


Fig. 7. Adsorption capacity of different gas ratio of CH_4/CO_2 in illite (a) 75 % $\text{CO}_2 + 25\% \text{CH}_4$; (b) 50 % $\text{CO}_2 + 50\% \text{CH}_4$; (c) 25 % $\text{CO}_2 + 75\% \text{CH}_4$.

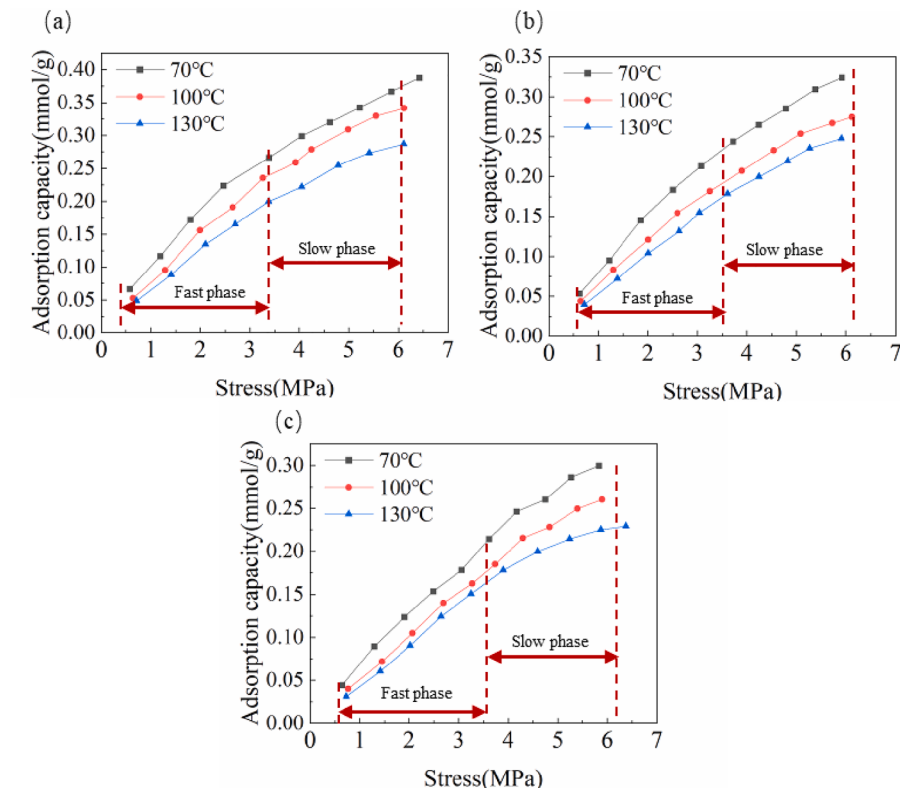


Fig. 8. Adsorption capacity of different gas ratio of CH_4/CO_2 in calcite (a) 75 % CO_2 + 25 % CH_4 ; (b) 50 % CO_2 + 50 % CH_4 ; (c) 25 % CO_2 + 75 % CH_4 .

3.2. CH_4/CO_2 competitive adsorption characteristics under different temperatures

Fig. 6 shows the adsorption capacities of montmorillonite for the CH_4/CO_2 gas mixture at different temperatures. When the CH_4/CO_2 ratio was determined, the total adsorption capacity of montmorillonite for the CH_4/CO_2 gas mixture decreased with the increase in temperature. For instance, the gas mixture was 75 % CO_2 + 25 % CH_4 , the adsorption capacity at each pressure point decreased with the increase in temperature; when the pressure is around 6 MPa, the adsorption capacities at 70°C, 100°C, and 130°C are 0.381 mmol/g, 0.332 mmol/g, and 0.284 mmol/g, respectively.

In Fig. 7, the adsorption capacities of illite for the CH_4/CO_2 gas mixture also decreased with the increase in temperature. For instance, when the gas mixture was 75 % CO_2 + 25 % CH_4 , and the pressure was around 6 MPa, the adsorption capacities at 70°C, 100°C, and 130°C were 0.085 mmol/g, 0.078 mmol/g, and 0.067 mmol/g, respectively.

As shown in Fig. 8, the adsorption capacities of calcite for the gas mixture was similar to those of the previous two minerals. Clearly, at the pressure of 0–6 MPa, the adsorption capacities of the three minerals for

the CH_4/CO_2 gas mixture at each pressure point obviously decreased with the increasing temperature (70–130°C). The adsorption capacity of calcite decreased from 0.145 mmol/g at 70°C to 0.132 mmol/g at 100°C and then to 0.118 mmol/g at 130°C, showing a phenomenon of the decreased adsorption capacity with the increase in temperature. Obviously, the low temperature was conducive to adsorption under this condition. In the adsorption processes of the three minerals, the increase in temperature will increase the molecular thermodynamics between the gases, and the Van der Waals force between the mineral surface and the gas molecules will also decrease, as a result, it will be easier for the gas molecules to escape the mineral adsorption sites.

In addition, under such condition, the three minerals all exhibited the characteristic of elevated pressure conductive to gas adsorption, but the adsorption growth rate gradually slowed down. The adsorption capacity growth trend of montmorillonite was roughly divided into two stages, including the rapid growth stage (0.5–3.3 MPa) and the slow growth stage (3.3–6 MPa). The adsorption capacity change rates of illite and calcite were similar, which were roughly divided into three stages, namely, the early pressure stage (0.5–2.3 MPa), the middle pressure stage (2.3–4.5 MPa) and the late pressure stage (4.5–6 MPa). The

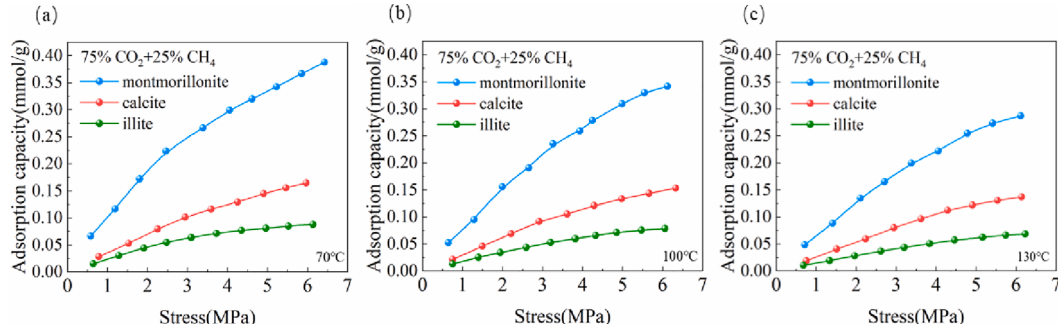


Fig. 9. Adsorption capacity curves of minerals under different temperature (a) 70°C (b) 100°C; (c) 130°C.

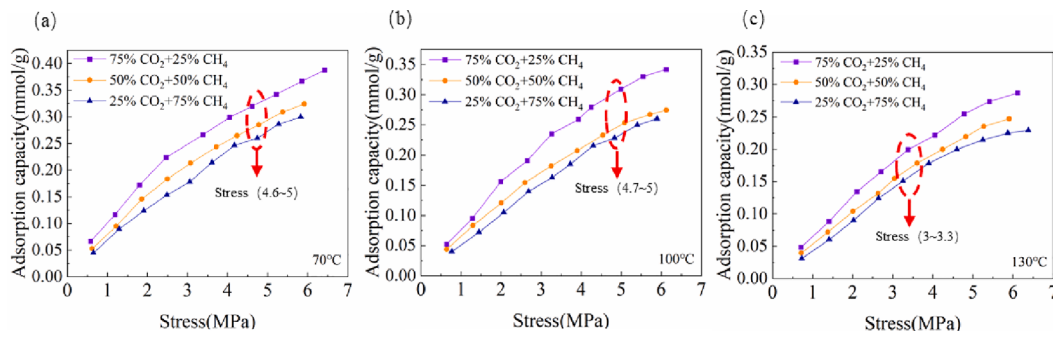


Fig. 10. Total adsorption capacities of montmorillonite for CH₄/CO₂ at different mixing gas ratios. (a) 70°C (b) 100°C; (c) 130°C.

adsorption capacity growth rates of illite and calcite demonstrated a gradually slowing trend in these three pressure stages.

The above results suggested that there were lots of adsorption sites and pore spaces on the surfaces of the three minerals, which could be quickly occupied by gas molecules under the low pressure condition. After the pressure critical points (3.3 MPa for montmorillonite, 2.3 MPa for illite and 4.5 MPa for calcite), the adsorption capacity increasing rates gradually slowed down. This is ascribed to the increasing contact probability between the gas mixture molecules and the mineral surface with the increasing pressure in the early stage, and the adsorption rates also gradually slowed down with the increasing pressure with the gradual decreases in the adsorption sites and storage spaces.

3.3. Influence of minerals properties on competitive adsorption

Under the same condition, the adsorption capacity curves of montmorillonite, illite and calcite (Fig. 9) showed that the total adsorption capacity of montmorillonite for the gas mixture was significantly greater than those of calcite and illite at different adsorption points, and that of illite was the smallest. For example, at the CO₂ ratio of 75 %, the temperature of 100°C, and the pressure of about 6 MPa, the adsorption capacity of montmorillonite was 0.332 mmol/g, that of calcite was 0.145 mmol/g, and that of illite was 0.078 mmol/g.

As observed from Fig. 9, under the high temperature condition, montmorillonite had the highest adsorption capacity for methane and carbon dioxide, followed by calcite. This is because that the montmorillonite has a far greater specific surface area than calcite and illite, which possesses more adsorption sites, reservoir space and there are more residual force fields on the surface to adsorb more gas. At the same time, montmorillonite has the greatest pore volume, which provides more gas storage space. Consequently, minerals with greater specific surface area and pore volume have greater adsorption capacities. In addition, the average pore size will affect the adsorption capacity of the minerals, and the smaller size of the pores makes it more difficult to adsorb. According to the average pore sizes of three minerals, the mineral adsorption capacity was negatively correlated with the average pore size.

Consistent with the analysis results of basic physical parameters of mineral samples, the specific surface area and total pore volume of montmorillonite and calcite were mainly derived from mesopores and micropores, which were the main spaces where methane/carbon dioxide gas were adsorbed in shale minerals. They had relatively large internal specific surface area and relatively small pore size, therefore, the adsorption potential fields of adjacent pore walls would be superimposed, leading to the greatly enhanced interaction force between the gas in the micropores and mesopores and the mineral surface. Moreover, the mesoporous structure could not only provide the gas adsorption sites, but also provide a larger gas storage space to ensure the free migration of gas molecules. The specific surface area and pore volume of illite were mainly composed of macropores and micropores, and the interaction between macropores and gas was small, giving rise to the relatively weak adsorption performance. Consequently, it can be seen that the adsorption performances of the three minerals under different complex conditions in the low pressure environment (0–6 MPa) satisfy the order of montmorillonite > calcite > illite.

3.4. Total adsorption capacities of CH₄/CO₂ under complex conditions

On the whole, at the same temperature, the adsorption capacities of the three minerals gradually increased with the increase in carbon dioxide concentration, and they showed a downward trend when the carbon dioxide concentration decreased.

Fig. 10 characterizes the total adsorption capacities of montmorillonite for CH₄/CO₂ at different mixing gas ratios. At 70°C and 6 MPa, the adsorption capacities of montmorillonite at three ratios (carbon dioxide concentrations from high to low) were 0.381 mmol/g, 0.328 mmol/g and 0.299 mmol/g, respectively, and the adsorption capacity gradually decreased. In general, the order of adsorption capacity of montmorillonite under these three gas ratios was 75 %CO₂ + 25 %CH₄ > 50 %CO₂ + 50 %CH₄ > 25 %CO₂ + 75 %CH₄. As seen from the red dashed line circle in the figure, at the pressure of 0.5–5 MPa, the adsorption capacities at diverse gas ratios gradually increased with the increase in pressure, but the adsorption capacity growth rate slowly decreased. When it exceeded 5 MPa, most of the adsorption curves had apparently

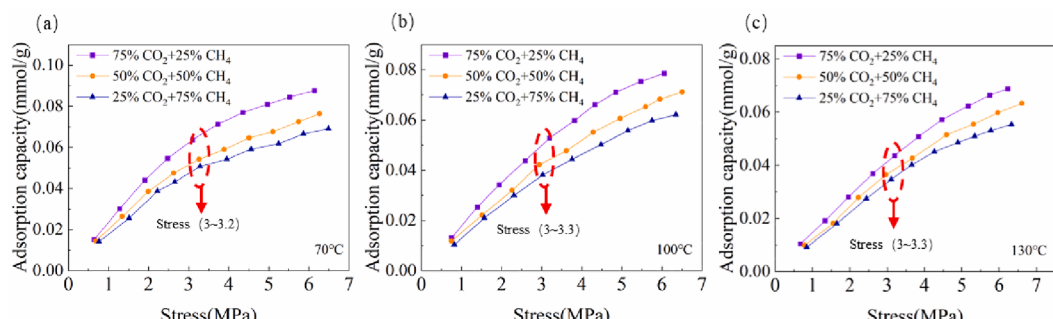


Fig. 11. Total adsorption capacities of illite for CH₄/CO₂ at different mixing gas ratios. (a) 70°C (b) 100°C; (c) 130°C.

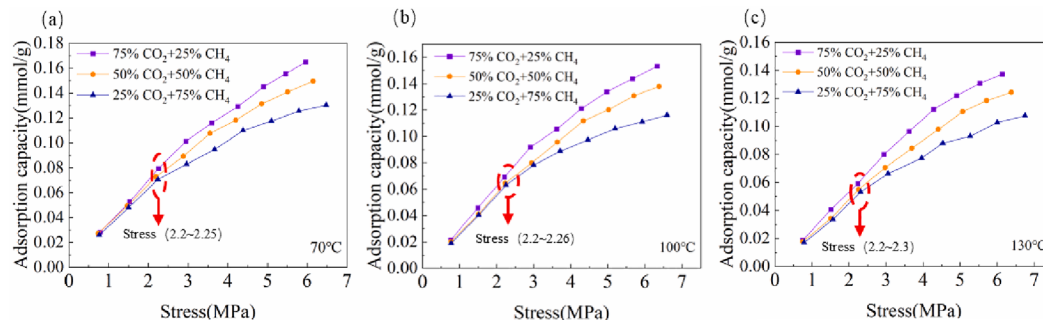


Fig. 12. Total adsorption capacities of calcite for CH_4/CO_2 at different mixing gas ratios. (a) 70°C (b) 100°C; (c) 130°C.

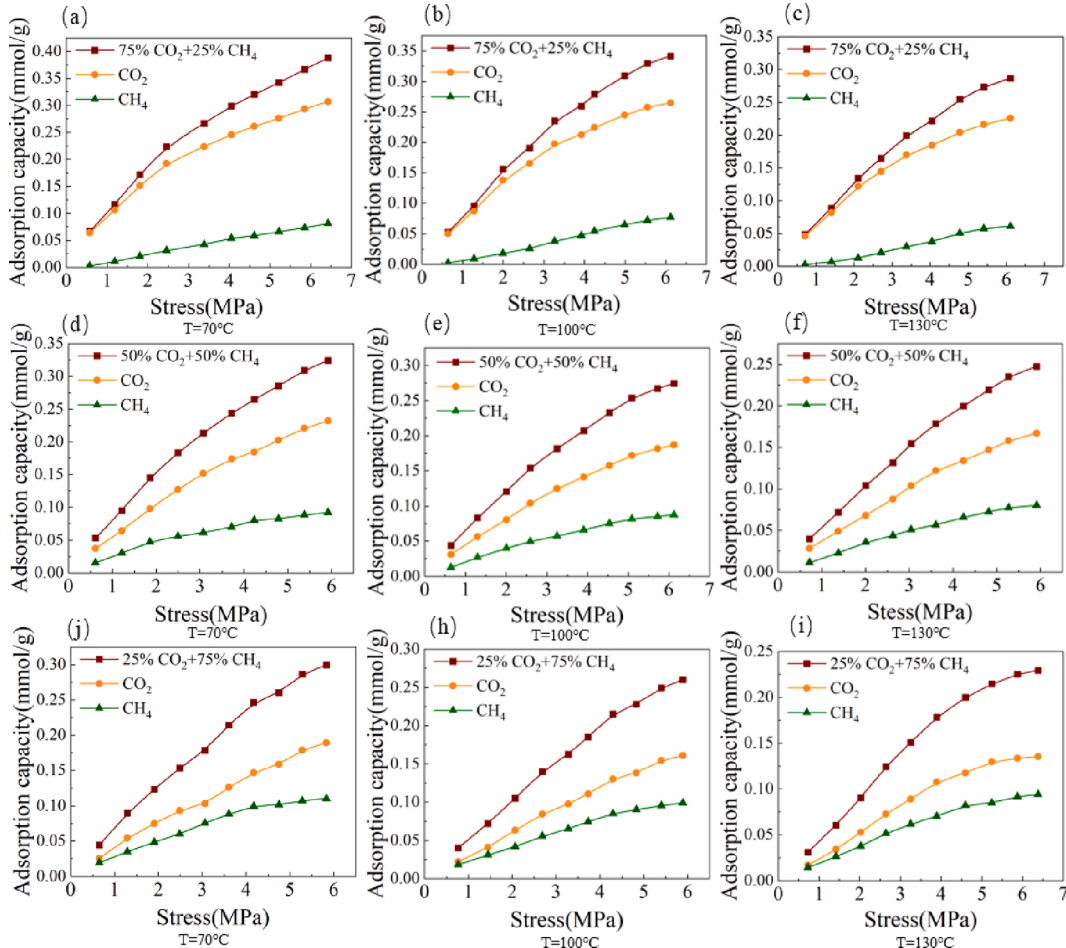


Fig. 13. Competitive adsorption behaviors of CH_4/CO_2 mixtures in montmorillonite under complex conditions (a) 75 % CO_2 + 25 % CH_4 , 70°C (b) 75 % CO_2 + 25 % CH_4 , 100°C; (c) 75 % CO_2 + 25 % CH_4 , 130°C; (d) 50 % CO_2 + 50 % CH_4 , 70°C (e) 50 % CO_2 + 50 % CH_4 , 100°C; (f) 50 % CO_2 + 50 % CH_4 , 130°C; (g) 25 % CO_2 + 75 % CH_4 , 70°C (h) 25 % CO_2 + 75 % CH_4 , 100°C; (i) 25 % CO_2 + 75 % CH_4 , 130°C.

decreased growth rate.

As shown in the Fig. 11, the adsorption capacity growth rate of illite increased rapidly at 0.5–3.3 MPa. After 3.3 MPa, the adsorption capacity growth rate decreased gradually. However, with the increase in pressure, there was a more obvious difference in the adsorption capacity caused by the change in the gas mixture concentration.

As for calcite (in Fig. 12), at the same temperature and 0.5–2.3 MPa, the adsorption capacity increased the fastest. At the pressure of 2.3–6 MPa, the difference in mineral adsorption capacity caused by gas mixture concentration was more obvious. For instance, at around 100 °C, 2.2 MPa, and CO_2 ratios of 75 %, 50 %, and 25 %, the adsorption capacities of calcite were 0.069 mmol/g, 0.065 mmol/g, and 0.062

mmol/g, respectively, with a minor difference in adsorption capacity. However, at around 5 MPa, the corresponding adsorption capacities of calcite were 0.130 mmol/g, 0.121 mmol/g, and 0.102 mmol/g, with a significant increase in difference. Such results suggest that in the low pressure environment, the increase in pressure is helpful to identify the effect of changes in CH_4/CO_2 concentration on the mineral adsorption capacity.

3.5. Competitive adsorption characteristics of CH_4/CO_2 under complex conditions

Fig. 13 presents the competitive adsorption behaviors of CH_4/CO_2

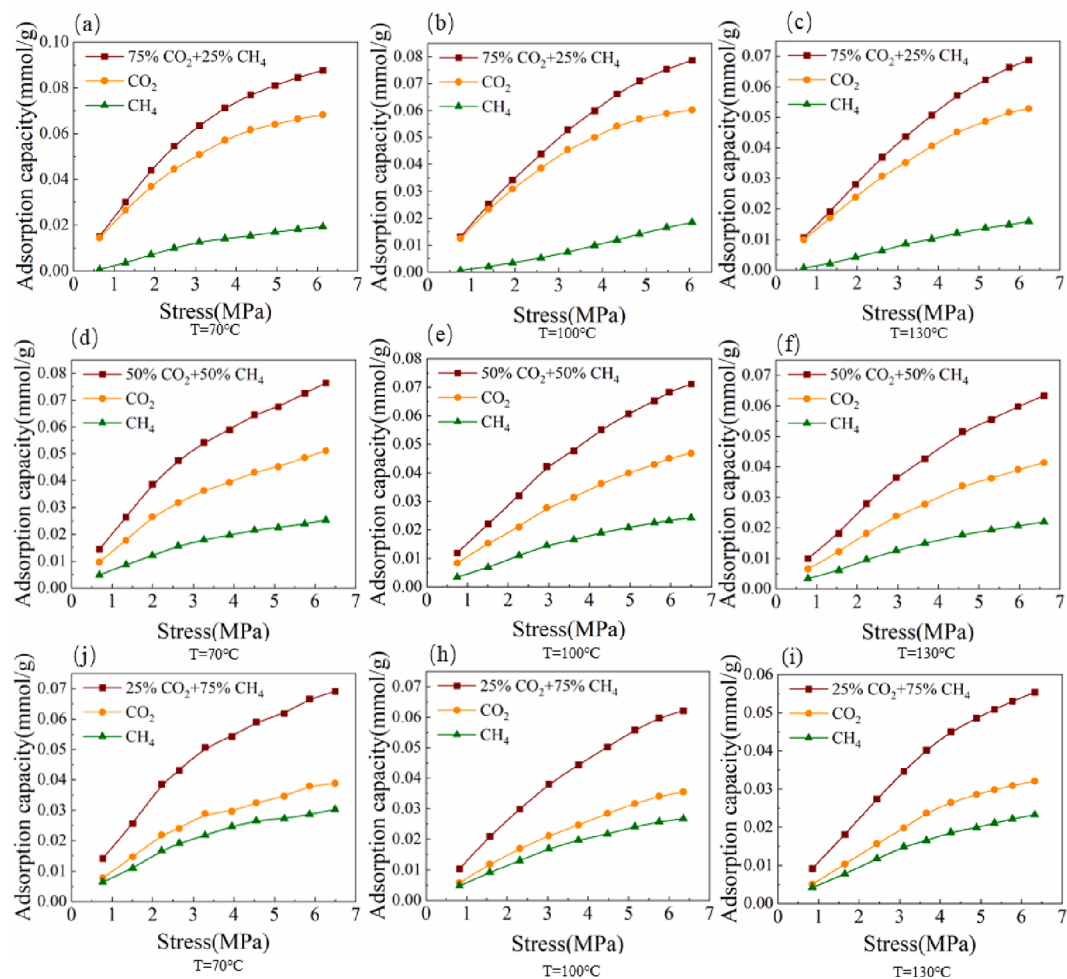


Fig. 14. Competitive adsorption behaviors of CH₄/CO₂ mixtures in illite under complex conditions (a) 75 %CO₂ + 25 %CH₄, 70°C (b) 75 %CO₂ + 25 %CH₄, 100°C; (c) 75 %CO₂ + 25 %CH₄, 130°C; (d) 50 %CO₂ + 50 %CH₄, 70°C (e) 50 %CO₂ + 50 %CH₄, 100°C; (f) 50 %CO₂ + 50 %CH₄, 130°C; (g) 25 %CO₂ + 75 %CH₄, 70°C (h) 25 %CO₂ + 75 %CH₄, 100°C; (i) 25 %CO₂ + 75 %CH₄, 130°C.

mixtures in montmorillonite under complex conditions. As observed from the figure, at the CO₂ ratio of 75 %, the overall adsorption capacity was more similar to the trend of CO₂ adsorption curve due to the higher CO₂ concentration. At the CO₂ ratios of 50 % and 25 %, the adsorption capacity of montmorillonite for CO₂ was also greater than that for CH₄, which is due to the greater interaction force between CO₂ and mineral surface. However, with the decrease in CO₂ concentration, the difference between the adsorption capacities for CH₄ and CO₂ gradually became smaller. For example, at 70°C and 6 MPa, the differences between the adsorption capacities for carbon dioxide and methane in the 75 %, 50 % and 25 %CO₂ mixtures were 0.22 mmol/g, 0.14 mmol/g and 0.079 mmol/g, respectively. This suggests that, with the decrease in CO₂ concentration, the competitive adsorption efficiency of CO₂ against CH₄ became lower and lower, and the mixture ratio with the best competitive effect was 75 %CO₂ + 25 %CH₄, followed by 50 %CO₂ + 50 %CH₄.

Fig. 14 presents the competitive adsorption behaviors of CH₄/CO₂ mixtures in illite under complex conditions. In this experiment, the adsorption of illite for CO₂ was always greater than that for CH₄. With the increase in CH₄ concentration, the adsorption advantage for carbon dioxide weakened; for instance, at around 100 °C and 6 MPa, the differences in adsorption capacities of CO₂ and CH₄ under CH₄ ratios of 25 %, 50 %, and 75 % were 0.042 mmol/g, 0.021 mmol/g, and 0.008 mmol/g, respectively.

Fig. 15 presents the competitive adsorption behaviors of CH₄/CO₂ mixtures in calcite. Similarly, the total adsorption capacity curve of calcite was closer to the adsorption curve of carbon dioxide, which also

showed a stronger adsorption capacity for carbon dioxide. In particular, at the carbon dioxide ratio of 75 % (at 70°C, 6 MPa), the adsorption capacities for carbon dioxide and methane were 0.130 mmol/g and 0.034 mmol/g, respectively. With the increase in carbon dioxide concentration, the difference between the adsorption capacities of calcite for carbon dioxide and methane also continued to increase. For instance, at 130°C and 6 MPa, the differences between the adsorption capacities for carbon dioxide and methane in the 75 %, 50 % and 25 %CO₂ mixtures were 0.091 mmol/g, 0.048 mmol/g, and 0.021 mmol/g, respectively, which showed a decreasing trend in sequence.

To sum up, the adsorption capacities of montmorillonite, illite and calcite for CO₂ in the competitive adsorption of the CH₄/CO₂ gas mixture were much higher than those for CH₄, and they had higher affinity for CO₂ at 70–130°C and 0–6 MPa. With the increase in CO₂ concentration, the adsorption capacities of the three minerals for the gas mixture increased, the total adsorption capacity curve was much closer to the CO₂ adsorption capacity curve, and the difference in the adsorption capacity for CH₄/CO₂ also increased with the increase in CO₂ concentration.

Meanwhile, within the range of 70–130°C and 0–6 MPa, under the same conditions, the total adsorption capacity of the three shale minerals for the gas mixture: montmorillonite > calcite > illite. For example, at 75 %CO₂, 100 °C, and the pressure of about 6 MPa, the adsorption capacities of montmorillonite, calcite, and illite were 0.332 mmol/g, 0.145 mmol/g, and 0.078 mmol/g, respectively, which is consistent with the analysis results of the basic physical parameters of

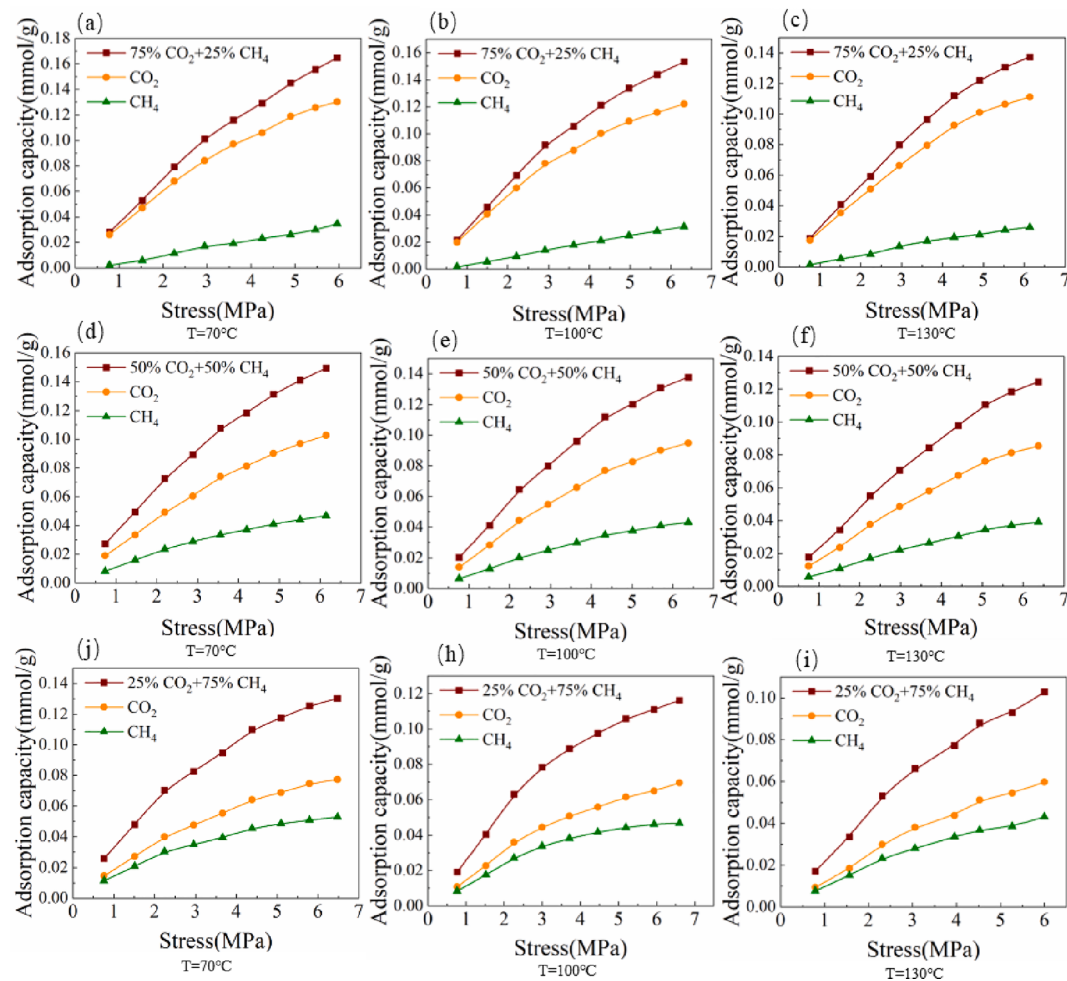


Fig. 15. Competitive adsorption behaviors of CH_4/CO_2 mixtures in calcite under complex conditions (a) 75 % CO_2 + 25 % CH_4 , 70°C (b) 75 % CO_2 + 25 % CH_4 , 100°C; (c) 75 % CO_2 + 25 % CH_4 , 130°C; (d) 50 % CO_2 + 50 % CH_4 , 70°C (e) 50 % CO_2 + 50 % CH_4 , 100°C; (f) 50 % CO_2 + 50 % CH_4 , 130°C; (g) 25 % CO_2 + 75 % CH_4 , 70°C (h) 25 % CO_2 + 75 % CH_4 , 100°C; (i) 25 % CO_2 + 75 % CH_4 , 130°C.

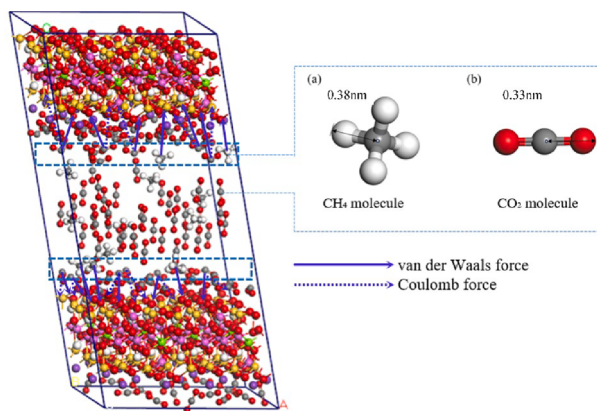


Fig. 16. Equilibrium configuration of calcite (50 % CO_2 + 50 % CH_4).

minerals mentioned above.

As shown in Fig. 16, as a linear molecule, CO_2 molecules had a slightly smaller aerodynamic diameter (0.33 nm), while CH_4 had a larger molecular diameter (0.38 nm). It means that CO_2 was more likely to enter and adhere onto the smaller pore structure on the mineral surfaces during the adsorption process, and occupy more adsorption sites, which resulted in the lower pore surface tension and adsorption capacity for external gases, thus reducing the adsorption for CH_4 . On the

other hand, the physical adsorption of minerals for gases was dominated by the interaction between the mineral surface and gas molecules. Methane was a non-polar molecule with Van der Waals force but no coulomb force. Compared with CH_4 , the CO_2 molecule had higher dipole moment and quadrupole moment, with both coulomb force and Van der Waals force, consequently, the interaction force between CO_2 molecule and the three shale minerals was much greater than that of CH_4 molecule, and desorption was not easy to take place.

In the actual mining of shale gas, the adsorption capacity may also be affected by other factors such as mineral water content, organic matter maturity and soluble component content, which will also be one of the future research works of the research group.

4. Conclusions

In this paper, based on the volumetric isothermal adsorption experiment, the competitive adsorption behaviors of several typical shale minerals under different burial depths and different mixing ratios of CH_4/CO_2 (75 % CO_2 + 25 % CH_4 ; 75 % CO_2 + 25 % CH_4 ; 50 % CO_2 + 50 % CH_4) were investigated; meanwhile, the competitive adsorption characteristics for CH_4/CO_2 under different temperature (70°C, 100°C, and 130°C) and pressure (0–6 MPa) conditions were explored, so as to provide basic data for the research on CO_2 displacement of shale gas technology in the low pressure environment. The main conclusions are drawn as follows:

When analyzing the basic physical parameters of the three shale

minerals, illite was mainly composed of micropores, macropores and lamellar fracture pores, with relatively simple pore structure. The pores of montmorillonite were mostly mesoporous. While the mesoporous structure of calcite was more complex, which was dominated by slit pores. The specific surface areas of the three shale minerals satisfied the order of montmorillonite > calcite > illite. Montmorillonite had a larger pore volume ($0.1885 \text{ cm}^3/\text{g}$), while calcite and illite had relatively smaller pore volumes. Micropores and mesopores contributed more to the pore structures and specific surface areas of the three minerals. Theoretically, the development degrees of specific surface area, pore volume and pore structure of minerals are proportional to their adsorption capacities.

In the isothermal adsorption experiment, at $70\text{--}130^\circ\text{C}$ and $0\text{--}6 \text{ MPa}$, under the same gas ratio condition, the adsorption capacities of montmorillonite, illite and calcite also increased with the increase in pressure, but the growth rate gradually decreased. Notably, the adsorption capacity of montmorillonite increased the fastest in the pressure range of $0.5\text{--}3.3 \text{ MPa}$. Whereas illite and calcite had the fastest growth rates in the range of $0.5\text{--}2.3 \text{ MPa}$. At $70\text{--}130^\circ\text{C}$, the adsorption capacities of the three minerals for the gas mixture decreased with the increasing temperature.

Under the same temperature and gas ratio conditions, the total adsorption capacities of the three shale minerals for the gas mixture satisfied the order of montmorillonite > calcite > illite, consistent with the analysis results of the basic physical parameters of the minerals. At the same time, montmorillonite, illite and calcite all exhibited stronger adsorption capacities for carbon dioxide (compared with methane), and the total adsorption capacity curves were closer to the carbon dioxide adsorption curve.

At the mixing gas ratios used in this experiment, the adsorption capacities of the three minerals for carbon dioxide were always greater than those for methane, and the difference in adsorption capacity between carbon dioxide and methane gradually increased with the increasing carbon dioxide concentration, proving that the increase in carbon dioxide concentration inhibited the adsorption of minerals for methane. The optimal mixing ratio for competitive adsorption is $75\% \text{ CO}_2 + 25\% \text{ CH}_4$, (montmorillonite, illite and calcite adsorption capacity: 0.332 mmol/g , 0.078 mmol/g and 0.145 mmol/g ; 100°C , 6 MPa) followed by $50\% \text{ CO}_2 + 50\% \text{ CH}_4$.

CRediT authorship contribution statement

Sen Tian: Writing – review & editing, Writing – original draft, Supervision, Project administration, Funding acquisition, Formal analysis, Data curation, Conceptualization. **Huimin Jia:** Writing – review & editing, Writing – original draft, Visualization, Formal analysis, Data curation, Conceptualization. **Zhaolong Ge:** Writing – original draft, Project administration, Funding acquisition, Formal analysis. **Guangjin Wang:** Writing – original draft, Project administration, Methodology, Funding acquisition. **Ruyi Bai:** Methodology, Investigation, Formal analysis.

Declaration of competing interest

The authors declare that they have no known competing financial interests or personal relationships that could have appeared to influence the work reported in this paper.

Acknowledgment

This work is supported by the National Natural Science Foundation of China (Grant No. 51904040), the project of Mangshi Huasheng Gold Mine Development Co., Ltd. (H20241326), the Fundamental Research Funds for the Central Universities (Grant Nos. 2020CDJQY-A045; 2020CDJ-LHZZ-003), and the Program for Changjiang Scholars and Innovative Research Team in University (Grant No. IRT_17R112). The

authors would like to acknowledge the colleagues from the State Key Laboratory of Coal Mine Disaster Dynamics and Control for their perspectives and suggestions related to data collection and statistical analysis.

Data availability

No data was used for the research described in the article.

References

- [1] Song R, Feng X, Wang Y, Sun S, Liu J. Dissociation and transport modeling of methane hydrate in core-scale sandy sediments: a comparative study. *Energy* 2021; 221:119890. <https://doi.org/10.1016/j.energy.2021.119890>.
- [2] Lei Q, Weng D, Guan B, Shi J, Cai B, He C, et al. Shale oil and gas exploitation in China: technical comparison with US and development suggestions. *Petrol Explor Dev* 2023;50:944–54. [https://doi.org/10.1016/S1876-3804\(23\)60440-9](https://doi.org/10.1016/S1876-3804(23)60440-9).
- [3] Ma H, Yang Y, Zhang Y, Li Z, Zhang K, Xue Z, et al. Optimized schemes of enhanced shale gas recovery by $\text{CO}_2\text{-N}_2$ mixtures associated with CO_2 sequestration. *Energ Convers Manage* 2022;268:116062. <https://doi.org/10.1016/j.enconman.2022.116062>.
- [4] Yang Y, Liu S, Ma H. Impact of unrecovred shale gas reserve on methane emissions from abandoned shale gas wells. *Sci Total Environ* 2024;913:169750. <https://doi.org/10.1016/j.scitotenv.2023.169750>.
- [5] He X, He G, Gao Y, Zhang L, He Q, Zhang P, et al. Progress in and research direction of key technologies for normal-pressure shale gas exploration and development. *Nat Gas Ind B* 2023;10:555–69. <https://doi.org/10.1016/j.ngib.2023.11.003>.
- [6] Zhang J, Xie Z, Pan Y, Tang J, Li Y. Synchronous vertical propagation mechanism of multiple hydraulic fractures in shale oil formations interlayered with thin sandstone. *J Petrol Sci Eng* 2023;220:111229. <https://doi.org/10.1016/j.petrol.2022.111229>.
- [7] Wang W, Wen J, Wang C, Gomari SR, Xu X, Zheng S, et al. Current status and development trends of CO_2 storage with enhanced natural gas recovery (CS-EGR). *Fuel* 2023;349:128555. <https://doi.org/10.1016/j.fuel.2023.128555>.
- [8] Li X, Chen D, Li Z, Liu S, Zhai M, Li Y, et al. Roadway portal and self-moving hydraulic support for rockburst prevention in coal mine and its application. *Phys Fluids* 2024;36(12):124136. <https://doi.org/10.1063/5.0243798>.
- [9] Feng Y, Xiao X, Wang E, Gao P, Lu C, Li G. Gas storage in shale pore system: a review of the mechanism, control and assessment. *Petrol Sci* 2023;20:2605–36. <https://doi.org/10.1016/j.petsci.2023.05.012>.
- [10] Hu C, Tan J, Lyu Q, Zhang Y. Evolution of organic pores in permian low maturity shales from the dalong formation in the sichuan basin: insights from a thermal simulation experiment. *Gas Sci Eng* 2024;121:205166. <https://doi.org/10.1016/j.jgsce.2023.205166>.
- [11] Tang C, Li B, Li J, Gao Z, Song H, Yang J. Study concerning the supercritical adsorption behavior of shale gas that analyzed different adsorption mechanisms. *Chem Eng Res Des* 2024;208:15–28. <https://doi.org/10.1016/j.cherd.2024.06.013>.
- [12] Mo C, Zhang G, Tang Y, Chen Z. Adsorption mechanism study of sour natural gas and sulfur in high-sulfur carbonate rock gas reservoirs. *Gas Sci Eng* 2024;125. <https://doi.org/10.1016/j.jgsce.2024.205290>.
- [13] Dai X, Tian S, He Y, Lu Y, Wang G. Methane/Carbon Dioxide Adsorption and Diffusion Performances at Different Mineral Compositions and Buried Depth Conditions. *Energy Fuels* 2021;35:15567–15578. <https://doi.org/10.1021/acs.energyfuels.1c01961>.
- [14] Ma X, Xie J, Yong R, Zhu Y, Zhao H, Krooss BM. Investigations on the methane sorption capacity of marina shales from Sichuan Basin. *China Int J Coal Geol* 2015; 146:104–17. <https://doi.org/10.1016/j.coal.2015.05.009>.
- [15] Miao F, Wu D, Liu X, Xiao X, Zhai W, Geng Y. Methane adsorption on shale under in situ conditions: Gas-in-place estimation considering in situ stress. *Fuel* 2022;308: 121991. <https://doi.org/10.1016/j.fuel.2021.121991>.
- [16] Liu S, Wang J, Li H, Liu J, Xu J, Sun W, et al. A generalized adsorption model of $\text{CO}_2\text{-CH}_4$ in shale based on the improved Langmuir model. *Fuel* 2025;379:132971. <https://doi.org/10.1016/j.fuel.2024.132971>.
- [17] Lu C, Xiao X, Xue Z, Chen Z, Dong Y, Feng Y, et al. Investigations of methane adsorption characteristics on marine-continental transitional shales and gas storage capacity models considering pore evolution. *Petrol Sci* 2024;21:2273–86. <https://doi.org/10.1016/j.petsci.2024.03.027>.
- [18] Li J, Yang X, Wang M, Zhao J. Quantum physisorption behavior of methane in nanoporous shales: Model and new mechanism. *Mar Petrol Geol* 2024;170. <https://doi.org/10.1016/j.marpetgeo.2024.107129>.
- [19] Chalmers RG, Bustin MR. The organic matter distribution and methane capacity of the lower cretaceous strata of Northeastern British Columbia. *Canada Int J Coal Geol* 2007;70(1–3):223–39. <https://doi.org/10.1016/j.coal.2006.05.001>.
- [20] Abdollahi R, Motahhari SM, Askari AA, Hematpur H, Zamani Z, Tirtashi RB, et al. A systematic step-wise approach for shale gas assessment in undeveloped prospects: a case study of Lurestan shale gas area in Iran. *Petrol Explor Dev* 2022; 49:596–604. [https://doi.org/10.1016/S1876-3804\(22\)60049-1](https://doi.org/10.1016/S1876-3804(22)60049-1).

- [22] Xie W, Wang M, Chen S, Vandeginste V, Yu Z, Wang H. Effects of gas components, reservoir property and pore structure of shale gas reservoir on the competitive adsorption behavior of CO₂ and CH₄. *Energy* 2022;254:124242. <https://doi.org/10.1016/j.energy.2022.124242>.
- [23] Hu K, Mischo H. High-pressure methane adsorption and desorption in shales from the Sichuan Basin. *Southwestern China Energy Fuels* 2020;34:2945–57. <https://doi.org/10.1021/acs.energyfuels.9b04142>.
- [24] Li Z, Wang S, Wei G, Wang H, Zhao H, Liang R. The seepage driving mechanism and effect of CO₂ displacing CH₄ in coal seam under different pressures. *Energy* 2024;293:130740. <https://doi.org/10.1016/j.energy.2024.130740>.
- [25] Zhang C, Yao Y, Swennen R, Zhang Y. Re-evaluating the methane adsorption behavior in shale kerogen: unifying experiment and molecular simulation. *Phys Fluids* 2024;36:022002. <https://doi.org/10.1063/5.0188365>.
- [26] Liu Y, Hou J, Wang C. Absolute adsorption of CH₄ on shale with the simplified local-density theory. *SPE J* 2020;25:212–25. <https://doi.org/10.2118/199344-PA>.
- [27] Chen M, Kang Y, Zhang T, Li X, Wu K, Chen Z. Methane adsorption behavior on shale matrix at in-situ pressure and temperature conditions: measurement and modeling. *Fuel* 2018;228:39–49. <https://doi.org/10.1016/j.fuel.2018.04.145>.
- [28] Li C, Li L, Kang T. Measurement and modeling of the adsorption isotherms of CH₄ and C₂H₆ on shale samples. *Rsc Adv* 2019;9:13705–13. <https://doi.org/10.1039/c9ra01432b>.
- [29] Huang L, Xiao Y, Yang Q, Chen Q, Zhang Y, Xu Z, et al. Gas sorption in shale media by molecular simulation: advances, challenges and perspectives. *Chem Eng J* 2024;487:150742. <https://doi.org/10.1016/j.cej.2024.150742>.
- [30] Deng J, Guo S, Wan J, Zhang L, Song H. Molecular dynamics of CH₄ adsorption and diffusion characteristics through different geometric shale kerogen nanopores. *Chem Eng J* 2024;500:156784. <https://doi.org/10.1016/j.cej.2024.156784>.
- [31] Pang Y, Chen S, Wang H. Predicting adsorption of methane and carbon dioxide mixture in shale using simplified local-density model: implications for enhanced gas recovery and carbon dioxide sequestration. *Energies* 2022;15:2548. <https://doi.org/10.3390/en15072548>.
- [32] Liu J, Wen Y, Yuan H, Jiang L, Liu Z, Chen Y, et al. Molecular simulation calculation method for shale gas adsorption in realistic shale model. *Geoenergy Sci Eng* 2023;222:211440. <https://doi.org/10.1016/j.geoen.2023.211440>.
- [33] Pang P, Han H, Hu L, Guo C, Gao Y, Xie Y. The calculations of pore structure parameters from gas adsorption experiments of shales: which models are better? *J Nat Gas Sci Eng* 2021;94:104060. <https://doi.org/10.1016/j.jngse.2021.104060>.
- [34] Xu Y, Lun Z, Wang H, Zhao C, Zhou X, Hu W, et al. Understanding roles of moisture in CO₂ adsorption and desorption hysteresis on deep gas-bearing shales under high temperature and pressure. *Sep Purif Technol* 2024;334:125970. <https://doi.org/10.1016/j.seppur.2023.125970>.
- [35] Villarroel-Rocha J, Barrera D, Sapag K. Introducing a self-consistent test and the corresponding modification in the Barrett, Joyner and Halenda method for pore-size determination. *Micropor Mesopor Mat* 2014;200:68–78. <https://doi.org/10.1016/j.micromeso.2014.08.017>.
- [36] Liu S, Sun H, Zhang D, Yang K, Li X, Wang D, et al. Experimental study of effect of liquid nitrogen cold soaking on coal pore structure and fractal characteristics. *Energy* 2023;275(7):127470. <https://doi.org/10.1016/j.energy.2023.127470>.
- [37] Li X, Chen D, Fu J, Liu S, Geng X. Construction and application of fuzzy comprehensive evaluation model for rockburst based on microseismic monitoring. *Appl Sci-Basel* 2023;13(21):12013. <https://doi.org/10.3390/app132112013>.
- [38] Tian S, Bai R, Zhao Y, Lu Y, Chen J, Wu S. Molecular simulation and experimental study on adsorption effect of CH₄/CO₂ in Shale Minerals. *Ind Eng Chem Res* 2023;63:818–32. <https://doi.org/10.1021/acs.iecr.3c03162>.
- [39] David C, Ramji K, Kishore P, Velappa JS, Yuvraj S. Post-deposition annealing influences of gas adsorption on semi-vertical β-FeOOH nanorods at room temperature: a scanning kelvin probe analysis. *Mat Sci Eng B-Adv* 2022;280:115694. <https://doi.org/10.1016/j.mseb.2022.115694>.
- [40] Zuo Z, Lu P, Zhu C, Ji X. SAFT2 equation of state for the CH₄-CO₂-H₂O-NaCl quaternary system with applications to CO₂ storage in depleted gas reservoirs. *Chem Geol* 2024;667:122328. <https://doi.org/10.1016/j.chemgeo.2024.122328>.
- [41] Feng Y, Xiao X, Gao P, Hu D, Liu R, Li G, et al. Water distribution in pore systems and its influences on gas-bearing property of deep shale: a case study of the Longmaxi Formation in the Luzhou area, southern Sichuan Basin. *Mar Petrol Geol* 2024;163:106805. <https://doi.org/10.1016/j.marpetgeo.2024.106805>.
- [42] Zhou Q, Zhu Z, Liu W, Lu H, Fan Z, Nie X, et al. Hydraulic fracturing behaviors of shale under coupled stress and temperature conditions simulating different burial depths. *783 779 Int J Min Sci Techno* 2024;34. <https://doi.org/10.1016/j.ijmst.2024.06.005>.